

# Dynamic Characteristics and Vibrational Response of a Capacitive Micro-Phase Shifter

M. Fathalilou<sup>1</sup>, M. Sadeghi<sup>1</sup>, S. Afrang<sup>2</sup>, G. Rezazadeh<sup>3,\*</sup>

<sup>1</sup>Mechanical Engineering Department, University of Tabriz, Iran

<sup>2</sup>Electrical Engineering Department, Urmia University, Iran

<sup>3</sup>Mechanical Engineering Department, Urmia University, Iran

Received 30 January 2011; accepted 3 March 2011

## ABSTRACT

The objective of this paper is to control the phase shifting by applying a bias DC voltage and changing the mechanical characteristics in electrostatically-actuated micro-beams. This problem can be more useful in the design of micro-phase shifters, which has not generally been investigated their mechanical behavior. By presenting a mathematical modeling, Galerkin-based step by step linearization method (SSLM) and Galerkin-based reduced order model have been used to solve the governing static and dynamic equations, respectively. The equilibrium positions or fixed points of the system have been determined and the calculated static and dynamic pull-in parameters have been validated by previous experimental and theoretical results and a good agreement has been achieved. The frequency response of the system has been studied and illustrated that changing applied bias DC voltage affects the resonance frequency and maximum amplitude of the system vibrations. Then, phase diagram of the system for various damping ratio and excitation frequencies has been gained. It has been shown that by changing the bias DC voltage applied on the electrostatically-actuated micro-beam, which can be used as a varactor in phase shifter circuit, the stiffness of the micro-beam changes and consequently the phase shifting can be controlled. Finally, effect of the geometrical and mechanical properties of the micro-beam on the value of the phase shifting has been studied.

© 2011 IAU, Arak Branch. All rights reserved.

**Keywords:** MEMS; Phase shifter; Micro-beam; Electrostatic; Pull-in phenomena.

## 1 INTRODUCTION

**M**ICROELECTROMECHANICAL systems (MEMS) are increasingly gaining popularity in modern technologies, such as atomic force microscope (AFM), sensing sequence-specific DNA, and detection of single electron spin, mass sensors, micro-pumps, chemical sensors, pressure sensors and phase shifters [1-3]. MEMS devices are generally classified according to their actuation mechanisms. Actuation mechanisms for MEMS vary depending on the suitability to the application at hand. The most common actuation mechanisms are electrostatic, pneumatic, thermal, and piezoelectric [4]. Electrostatically actuated devices form a broad class of MEMS devices due to their simplicity, as they require few mechanical components and small voltage levels for actuation [4]. These devices are fabricated, to some extent, in a more mature stage than some other MEMS devices. As the microstructure is balanced between electrostatic attractive force and mechanical (elastic) restoring force, both electrostatic and elastic restoring force are increased when the electrostatic voltage increases. When the voltage reaches the critical value, pull-in instability happens. Pull-in is the point at which the elastic restoring force can no longer balance the electrostatic force. Furthermore, increasing the voltage will cause the structure to have dramatic displacement jump which causes structure collapse and failure. Pull-in instability is a snap-through like behavior and

\* Corresponding author. Tel.: +98 914 145 1407

E-mail address: g.rezazadeh@urmia.ac.ir (GH. Rezazadeh).

it is saddle-node bifurcation type of instability. In some devices such as micro-mirrors and micro-resonators, the designer avoids this instability to achieve stable motions, while in switching applications the designer exploits this effect to optimize device's performance. Some previous studies predicted pull-in phenomena based on static analysis by considering static application of a DC voltage [5, 6]. Beside the static pull-in, some researches introduced a dynamic pull-in voltage [7-9]. Dynamic pull-in voltage is defined as a step DC voltage that when is applied suddenly, leads to the instability of the system [7]. Phase shifters are key components of many communication and sensor systems. They are used to delay the phase or timing of a sinusoidal wave. Phase shifters have many applications in instrumentation systems and wireless communication circuits but are most significantly used in phased array antennas for telecommunications and radar applications [10].

Prior to the advent of electronically variable phase shifters almost all phase shifters, both fixed and variable, were mechanical [10, 11]. Electronic phase shifters assumed special significant because of their potential utility and volume requirement in phased array antenna systems for inertial less scanning. With the first demonstration of ferrite phase shifters for phase array scanning, there began a new era of ferrite phase shifter technology [12]. Another important class of phase shifters employing p-i-n diodes as electronic switches for phase shift control came into existence [13]. In the meantime, particularly since the 1980s, several other types of electronic phase shifting devices have emerged; the most important ones being the GaAs FET active phase shifters [14]. With the advent of monolithic microwave integrated circuit (MMIC) technology, MMIC phase shifters employing MESFETs and varactors as electronic control elements have been made possible as well [15].

MEMS bridges have recently been developed for MEMS phase shifters. The advantage of using MEMS over solid state devices is their low loss and wider band performance. Most of the microelectromechanical systems (MEMS) phase shifters developed today are based on established designs except that the solid state switch is replaced by a MEMS bridge. Depending on the type of operation, phase shifters can be categorized as analog or digital. The analog phase shifter results in a continuously variable phase shift, from 0 to 360° [16]. Digital phase shifters provide a discrete set of phase delays and are usually built using switches [17, 18]. In other classification, all kind of phase shifters are based on three main techniques: 1) switched-delay line [19], 2) reflect line [20], and 3) distributed loaded-line. This work presents analog type Distributed MEMS transmission lines (DMTL) phase shifter.

In spite of the many research about the phase shifters, effects of the mechanical and geometrical parameters on the behavior of phase shifters had not been studied generally. In this paper, theoretically, the mechanical behavior of an electrostatically-actuated micro-beam is studied which can be used as a varactor in phase shifter. By applying a mathematical modeling and numerical solution, the static and dynamic characteristics of the system is studied. The frequency response of the system for various bias DC voltages is plotted and effects of the bias DC voltage on the resonance frequency and vibration amplitude are studied. The phase shifting is investigated for various frequencies and different damping ratios. Then, the phase shifting is controlled by applying a bias DC voltage on the varactor of the phase shifter. Finally, effects of geometry of the varactor on the phase shifting are shown.

## 2 MODEL DESCRIPTION

Fig. 1 shows a schematic view of a simple RLC circuit of a phase shifter. In this paper, it is focused on the mechanical behavior of the varactor of Fig. 1 shown clearly in Fig. 2.

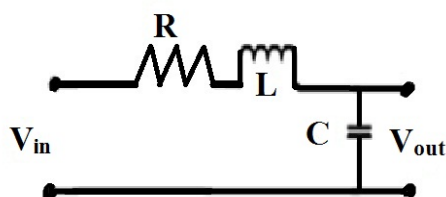


**Fig. 1**  
A schematic view of a RLC circuit.

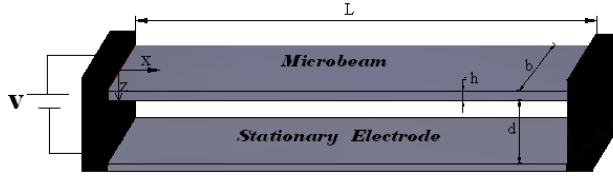


**Fig. 2**  
An electrostatically actuated fixed-fixed micro-beam.

The governing equation of motion for the transverse displacement of the beam  $w(x,t)$  actuated by an electrostatic load of voltage  $V(t)$  is written as [3]:

$$EI \frac{\partial^4 w}{\partial x^4} + \rho b h \frac{\partial^2 w}{\partial t^2} + c \frac{\partial w}{\partial t} = \frac{\epsilon b}{2} \left( \frac{V(t)}{d - w(x,t)} \right)^2 \quad (1)$$

where  $E$  is the Young's modulus.  $I = bh^3 / 12$  is the effective moment of inertia of the cross-section which is wide relative to thickness and width,  $\rho$  is density,  $\epsilon$  and  $d$  are the dielectric constant of the gap medium and initial gap, respectively. The micro-beam is subject to a viscous damping, which can be due to squeeze-film damping. This effect is approximated by an equivalent damping coefficient  $c$  per unit length [21]. The boundary conditions of the micro-beam are written as follow:

$$w(0,t) = w(L,t) = 0, \quad \frac{\partial w}{\partial x}(0,t) = \frac{\partial w}{\partial x}(L,t) = 0 \quad (2)$$

For convenience in analysis, this equation can be non-dimensionalized. In particular, both the transverse displacement,  $w$ , and the spatial coordinate,  $x$ , are normalized by characteristic lengths of the system and the gap size and beam length, respectively, according to:  $\hat{w} = w/d$  and  $\hat{x} = x/l$ . Time is non-dimensionalized by a characteristic period of the system according to:  $\hat{t} = t/t^*$  with  $t^* = (\rho b h L^4 / \tilde{E} I)^{1/2}$ . Substituting these parameters into Eq. (1), the following non-dimensional equation is obtained:

$$\frac{\partial^4 \hat{w}}{\partial \hat{x}^4} + \frac{\partial^2 \hat{w}}{\partial \hat{t}^2} + \hat{c} \frac{\partial \hat{w}}{\partial \hat{t}} = \alpha \left( \frac{\hat{V}(t)}{1 - \hat{w}(\hat{x}, \hat{t})} \right)^2 \quad (3)$$

The geometrical parameter,  $\alpha$  and non-dimensional damping coefficient,  $\hat{c}$  appeared in Eq. (3) are:

$$\alpha = \frac{6\epsilon L^4}{\tilde{E} h^3 d^3}, \quad \hat{c} = \frac{12cL^4}{\tilde{E} b h^3 t^*} \quad (4)$$

### 3 NUMERICAL SOLUTION

#### 3.1 Static analysis

In the static analysis, there are no time derivatives, so using Eq. (3) the governed equation describing the static deflection of the micro-beam can be obtained as follow:

$$L(\hat{w}_s, V) = \frac{d^4 \hat{w}_s}{d\hat{x}^4} - \alpha \left( \frac{\hat{V}}{1 - \hat{w}_s(\hat{x})} \right)^2 = 0 \quad (5)$$

where the  $\hat{w}_s(\hat{x})$  for a fixed-fixed end micro-beam must be satisfied same boundary condition as mentioned in Eq. (2). Due to the nonlinearity of derived static equation, the solution is complicated and time consuming. Direct

applying the Galerkin method or finite difference method creates a set of nonlinear algebraic equation. In this paper, a method is used to solve it which consists of two steps. In first step, linearization method (SSLM) [22] is used gradually and in second step, Galerkin method for solving the linear obtained equation is applied. For using the SSLM, it is supposed that  $\hat{w}_s^k$  is the displacement of beam due to the applied voltage  $V^k$ . Therefore, by increasing the applied voltage to a new value, the displacement can be written as:

$$\hat{w}_s^{k+1} = \hat{w}_s^k + \delta\hat{w} = \hat{w}_s^k + \psi(\hat{x}) \tag{6}$$

when

$$V^{k+1} = V^k + \delta V \tag{7}$$

Therefore, Eq. (5) can be rewritten as follow:

$$\frac{d^4 \hat{w}_s^{K+1}}{d\hat{x}^4} - \alpha \left( \frac{V^{K+1}}{1 - \hat{w}_s^{K+1}} \right)^2 = 0 \tag{8}$$

By considering small value of  $\delta V$ , it is expected that  $\psi$  would be small enough, hence using of Calculus of Variation Theory and Taylor's series expansion about  $\hat{w}_s^k$  and applying the truncation to first order of it for suitable value of  $\delta V$ , it is possible to obtain desired accuracy. The linearized equation to calculate  $\psi$  can be expressed as:

$$L(\psi) = \frac{d^4 \psi}{d\hat{x}^4} - 2\alpha \frac{(V^k)^2}{(1 - \hat{w}_s^k)^3} \psi - 2\alpha \frac{V^k \delta V}{(1 - \hat{w}_s^k)} = 0 \tag{9}$$

The obtained linear differential equation is solved by Galerkin based on reduced order model. Based on  $\psi(\hat{x})$  function spaces can be expressed as:

$$\psi(\hat{x}) = \sum_{j=1}^{\infty} a_j \varphi_j(\hat{x}) \tag{10}$$

where  $\varphi_i(\hat{x})$  is the  $i$ th shape function that satisfies the boundary conditions. The unknown  $\psi(\hat{x})$  is approximated by truncating the summation series to a finite number,  $n$ :

$$\psi_n(\hat{x}) = \sum_{j=1}^n a_j \varphi_j(\hat{x}) \tag{11}$$

By substituting the Eq. (11) into Eq. (9), and multiplying by  $\varphi_i(\hat{x})$  as a weight function in Galerkin method and then integrating the outcome from  $\hat{x} = 0$  to 1, the Galerkin based reduced-order model is generated.

### 3.2 Dynamic analysis

In the dynamic analysis, it is considered that the micro-beam is deflected by a bias DC voltage,  $V_{DC}$  and then the dynamic characteristics and forced response of the system considered about these conditions. So, total deflection of the micro-beam consists of two parts as:

$$\hat{w}(\hat{x}, \hat{t}) = \hat{w}_s(\hat{x}) + \hat{w}_d(\hat{x}, \hat{t}) \tag{12}$$

$\hat{w}_s(\hat{x})$  introduces the static deflection of the beam and  $\hat{w}_d(\hat{x}, \hat{t})$  denotes the dynamic deflection about  $\hat{w}_s(\hat{x})$ . Because of the applied AC voltage in the model which is small enough than bias DC voltage  $V_d \ll V_s$  by linearizing Eq. (8) about calculated  $\hat{w}_s(\hat{x})$  small linear vibrations are studied by the following equation:

$$\frac{\partial^4 \hat{w}}{\partial \hat{x}^4} + \frac{\partial^2 \hat{w}}{\partial \hat{t}^2} + \beta \frac{\partial \hat{w}}{\partial \hat{t}} = \frac{\alpha(V_s + V_d)^2}{(1 - \hat{w})^2} = \frac{\alpha V_s^2}{(1 - w_s)^2} + \frac{2\alpha V_s}{(1 - w_s)^2} \delta V + \frac{2\alpha V_s^2}{(1 - w_s)^3} \delta w \quad (13)$$

where  $\delta V = V_d$  and  $\delta w = w_d$ . The  $V_d$  is small AC voltage and equal to  $V_0 \sin(\omega t)$  and  $\omega$  is excitation frequency. Subtracting Eq. (5), the linearized equation of motion about equilibrium position can be obtained in the following form:

$$\frac{\partial^4 \hat{w}_d}{\partial \hat{x}^4} + \frac{\partial^2 \hat{w}_d}{\partial \hat{t}^2} + \hat{c} \frac{\partial \hat{w}_d}{\partial \hat{t}} - \frac{2\alpha V_s^2}{(1 - w_s)^3} w_d = \frac{2\alpha V_s V_0 \sin(\omega t)}{(1 - w_s)^2} \quad (14)$$

In order to solve this equation, a Galerkin based reduced order model can be used [23]. So  $\hat{w}_d$  can be expressed as:

$$\hat{w}_d(\hat{x}, \hat{t}) = \sum_{j=1}^{\infty} T_j(\hat{t}) \varphi_j(\hat{x}) \quad (15)$$

where  $\varphi_j(\hat{x})$  is the  $j$ th shape function that satisfies the boundary conditions. The unknown  $\hat{w}_d(\hat{x}, \hat{t})$  can be approximated by truncating the summation series to a finite number,  $N$ :

$$\hat{w}_d(\hat{x}, \hat{t}) = \sum_{j=1}^N T_j(\hat{t}) \varphi_j(\hat{x}) \quad (16)$$

In this paper,  $\varphi_j(\hat{x})$  is selected as the  $j$ th un-damped linear mode shape of the straight micro-beam. By substituting the Eq. (16) into Eq. (14) and multiplying by  $\varphi_i(\hat{x})$  as a weight function in Galerkin method and then integrating the outcome from  $\hat{x} = 0$  to 1; the Galerkin based reduced order model is generated as:

$$\sum_{j=1}^n M_{ij} \ddot{T}_j(\hat{t}) + \sum_{j=1}^n C_{ij} \dot{T}_j(\hat{t}) + \sum_{j=1}^n (K_{ij}^{mech} - K_{ij}^{elec}) T_j(\hat{t}) = F_i \sin(\omega t) \quad (17)$$

where  $\bar{M}, \bar{C}, \bar{K}^{mech}$  and  $\bar{K}^{elec}$  are mass, damping, mechanical and electrical stiffness matrices, respectively. Also  $\bar{F}$  introduces the forcing vector. The mentioned matrices and vector are given by:

$$M_{ij} = \int_0^1 \varphi_i \varphi_j d\hat{x}, \quad C_{ij} = \hat{c} \int_0^1 \varphi_i \varphi_j d\hat{x}, \quad \beta K_{ij}^{elec} = \int_0^1 \frac{2\alpha V_s^2}{(1 - w_s)^3} \varphi_i \varphi_j d\hat{x}, \quad K_{ij}^{mech} = \int_0^1 \varphi_i \varphi_j^{iv} d\hat{x} \quad (18)$$

$$F_i = \int_0^1 \frac{2\alpha V_s V_0 \sin(\omega t)}{(1 - w_s)^2} \varphi_i d\hat{x}$$

The same procedure is used to study the response of the system to the step DC voltage, where the Eq. (17) is written as follow:

$$\sum_{j=1}^n M_{ij} \ddot{T}_j(\hat{t}) + \sum_{j=1}^n C_{ij} \dot{T}_j(\hat{t}) + \sum_{j=1}^n K_{ij}^{mech} T_j(\hat{t}) = F_i \tag{19}$$

where  $F$  introduces the forcing vector as follow:

$$F_i = \int_0^1 F(V, \hat{w}) \phi_i d\hat{x}, \quad i, j = 1, \dots, n \tag{20}$$

Eq. (20) can be integrated over time where  $\hat{w}(\hat{x}, \hat{t})$  in each time step of integration take the value of previous step. By applying the procedures mentioned, the static and dynamic instabilities and frequency response of the system are gained.

### 3.3 Phase diagram

Using the Kirchhoff low, the governing electrical equations for the input and output circles in Fig. 1 are written as following, respectively:

$$RI + L \frac{dl}{dt} + \frac{1}{c} \int Idt = V_{in} \tag{21}$$

$$\frac{1}{c} \int Idt = V_{out} \tag{22}$$

Due to very small value of the  $V_o$ , the variation of the capacitance of the varactor with the applied harmonic voltage is neglected and so for a given combination of DC and AC voltages, the  $c$  is considered constant. By solving this problem in frequency domain and applying the mechanical-electrical simulation, the phase shifting between input and output voltages is obtained as follow:

$$\phi = \tan^{-1} \frac{C\omega}{K - M\omega^2} \tag{23}$$

As shown in this equation, the phase shifting is a function of the equivalent mass,  $M$ , damping,  $C$ , total stiffness,  $K$  and excitation frequency,  $\omega$ .

## 4 RESULTS AND DISSCUSSION

For verification of our numerical solution of the static section it is considered a micro-beam with the geometrical and material properties listed in Table 1 [4].

**Table 1**  
Values of design variables

Design Variable	Value
$b$	50 $\mu\text{m}$
$h$	3 $\mu\text{m}$
$d$	1 $\mu\text{m}$
$E$	169 GPa
$\rho$	2331 $\text{kg/m}^3$
$\varepsilon$	8.85 PF/m
$\nu$	0.06

**Table 2**  
Comparison of the Pull-in Voltages for the fixed-fixed micro-beam

	Residual stress (MPa)	Our results	Energy model[24]	MEMCAD[24]
$L=350$	0	20.1V	20.2V	20.3V
	100	35.3V	35.4V	35.8V
	-25	13.8V	13.8V	13.7V
$L=250$	0	39.5V	39.5V	40.1V
	100	57.3V	56.9V	57.6V
	-25	33.4V	33.7V	33.6V

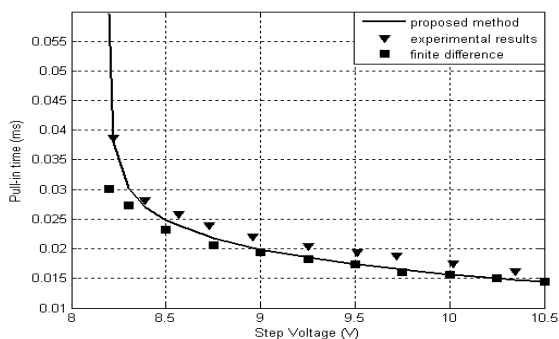


**Fig. 3**  
Comparison of the pull-in times for no damping case and no stretching effect.

In Table 2 it is compared the calculated pull-in voltage to the results of the previous works for the fixed-fixed micro-beam with properties listed in Table 1. It is shown that the calculated pull-in voltages are in good agreement with those existing in the previous works. For validation of results of the dynamic analysis with results of the previous works, a fixed-fixed micro-beam is considered which has the specifications of the pressure sensor used by Hung and Senturia [25]:

$$E = 149 \text{ GPa}, \quad \rho = 2330 \text{ kg/m}^3, \quad L = 610 \text{ }\mu\text{m}, \quad b = 40 \text{ }\mu\text{m}, \quad h = 2.2 \text{ }\mu\text{m}, \quad d = 2.3 \text{ }\mu\text{m}$$

Because  $h$  is given as a nominal value, it is modified to match the experimental pull-in voltage. Accordingly, thickness is obtained  $h = 2.135 \text{ }\mu\text{m}$ . They have considered a residual stress of  $-3.7 \text{ MPa}$ . In Fig. 3, the calculated pull-in time obtained using proposed method is compared to the theoretical and experimental results of Hung and Senturia for various values of step DC voltage. The pull-in time is found by monitoring the beam response over time for a sudden rise in the displacement; at that point, the time is reported as the pull-in time [21]. As Fig. 2 illustrates, calculated results are in excellent agreement with the theoretical and experimental results. It is shown that for no damping case before  $V = 8.18 \text{ V}$  the pull in instability do not occur, so this step DC voltage can be introduced as “dynamic pull-in voltage” for the micro-beam. In next sections, the micro-beam is considered with following properties:

$$L = 610 \text{ }\mu\text{m}, \quad b = 40 \text{ }\mu\text{m}, \quad h = 2 \text{ }\mu\text{m}, \quad d = 1.5 \text{ }\mu\text{m}, \quad E = 169 \text{ Gpa}, \quad \rho = 2331 \text{ kg/m}^3$$

The pull-in voltage for this system is  $6.65 \text{ V}$ . Fig. 4 illustrates the equilibrium positions of the fixed-fixed micro-beams versus applied voltage. As shown in this figure, for a given DC voltage the micro-beam has three fixed points or equilibrium positions. Fig. 5 shows phase portrait of the micro-beam for a given voltage with various initial conditions. Based on Fig. 5, it is found that for a given voltage the first equilibrium position is a stable centre, the second is a unstable saddle-node and the third is a mathematically stable centre but physically impossible due to the existence of the substrate. As shown in this figure, there are two basins of attraction of stable centers and a basin of repulsion of unstable saddle node. The first basin of attraction of the first stable center is bounded by a closed orbit and the second basin of attraction of the second stable is an unbounded region. Depending on the location of the initial condition, the system can be stable or unstable.

In addition, as shown, in Fig.4 in the state-control space, the stable and unstable branches of the fixed points, with increasing applied voltage, meet together at a saddle-node bifurcation point. The voltage corresponding to the saddle-node bifurcation point is a critical value, which is known as static pull-in voltage in the MEMS Literature. In other words, when the applied voltage equal to the static pull-in voltage there is no any basin of stable attractors on the upper side of the substrate and the micro-beam is unstable for every initial condition.

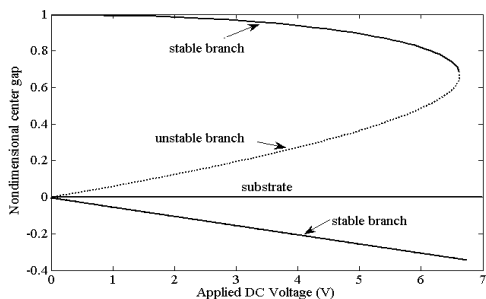


**Fig. 4**  
Variation of the center gap of the micro-beam with applied DC voltage.

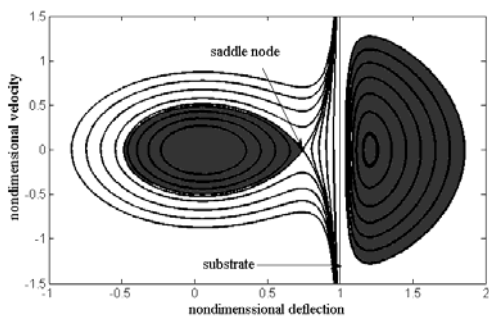


**Fig. 5**  
Phase portrait of the gold micro-beam for various initial conditions.

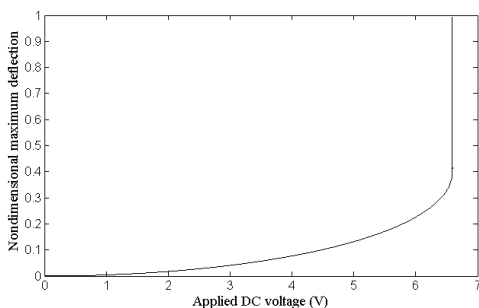


**Fig. 6**  
Maximum deflection of the micro-beam versus applied bias DC voltage.

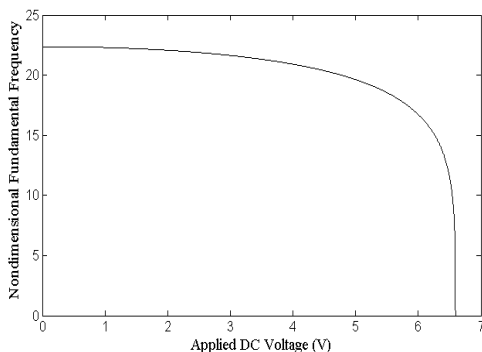


**Fig. 7**  
Variation of the fundamental frequency with bias DC voltage.



Figs. 6 and 7 show the variation of the maximum deflection and fundamental frequency of the system versus applied bias DC voltage, respectively. It is shown that the fundamental frequency of the system decreases by bias DC voltage and so at the pull in voltage divergence instability occurs and the frequency becomes zero. In Fig. 8, frequency response of the system for fundamental mode shape and various applied bias DC voltages is plotted. In this figure, amplitude of the harmonic voltage,  $V_0$  and non-dimensional damping ratio,  $\xi$  are considered  $0.001V$  and  $0.01$ , respectively. As shown, by increasing the bias DC voltage diagram shifts up. This is due to the decrease in stiffness of the system. In Fig. 9, the phase diagram of the system for un-deflected position is plotted. It is shown that by increasing the damping ratio, the phase shifting between the input and output voltages shifts up and down before and after the resonance frequency, respectively. In this section, it is illustrated that by applying a bias DC voltage on the system, the phase shifting between the input and output voltages can controlled.

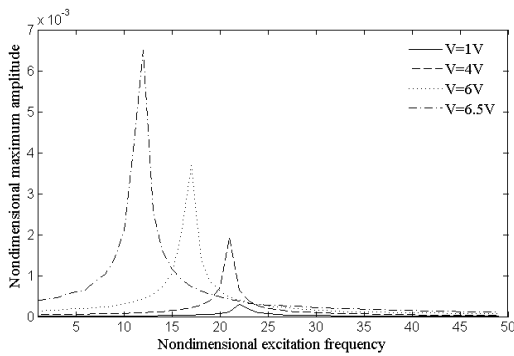


**Fig.8**  
The frequency response of the system for various applied bias DC voltage,  $V_0=0.001V$  and  $\xi = 0.01$ .

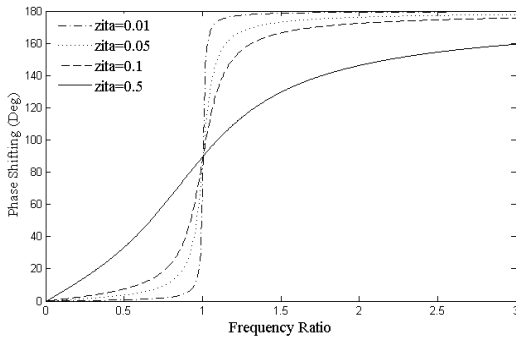


**Fig. 9**  
The phase diagram of the system for various damping ratios.

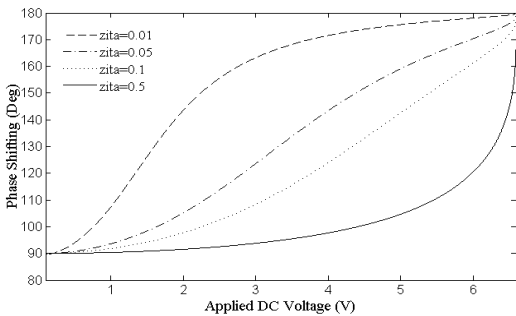


**Fig. 10**  
The phase shifting versus applied bias DC voltage for various damping ratios.

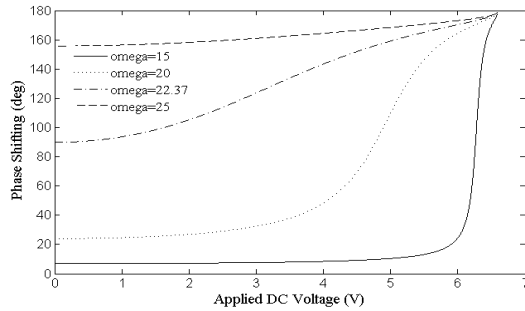


**Fig. 11**  
The phase shifting versus applied bias DC voltage for various excitation frequencies.

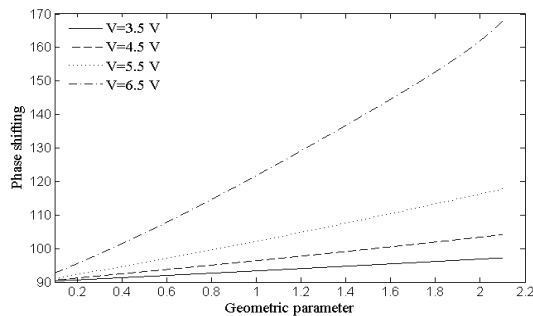


**Fig. 12**  
The phase shifting versus the geometrical parameter,  $\alpha$  for various bias DC voltage and non-dimensional resonance frequency.

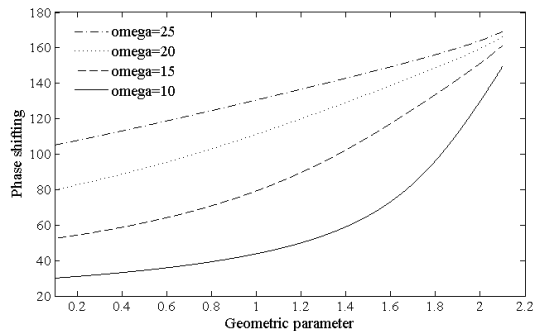


**Fig. 13**  
The phase shifting versus the geometrical parameter,  $\alpha$  for various excitation frequency and bias DC voltage of 6.5 V.

In Fig. 10, the effect of the bias DC voltage on the phase shifting for various damping ratios and resonance frequency ( $\omega=22.37$ ) is shown. Fig. 11 shows the phase shifting versus applied bias DC voltage for various excitation frequencies and a damping ratio of 0.05. It is shown that for the excitation frequencies which are lower than resonance frequency, the magnitude of the phase shifting is higher than other frequencies. In Fig. 12, the effect of the geometry of the micro-beam on the phase shifting for non-dimensional excitation frequency of 22.37 is shown. As illustrated, by increasing the geometrical parameter of the beam the phase shifting increases. This is due to decrease the stiffness of the system. Also, the rate of this increasing grows at higher bias DC voltages. This problem is shown for various excitation frequencies and applied bias DC voltage of 6.5 V in Fig. 13. It can be shown that the rate of increasing in phase shifting, especially at higher geometrical parameter, is higher for lower excitation frequencies.

## 5 CONCLUSIONS

The effects of mechanical and geometrical properties of an electrostatically actuated micro-beam- which can be used as a varactor in phase shifters, on the value of phase shifting between input and output voltages were investigated in the present work. By presenting a mathematical modeling and numerical solution, static and dynamic pull-in

voltages of the system were calculated and compared to previous results. Frequency response of the system for various applied bias DC voltages was plotted and shown that changing the bias DC voltage affects the resonance frequency and vibration amplitude of the system. It was illustrated that applying a bias DC voltage on the system, reduces the stiffness of system and so increases the value of phase shifting. This problem was shown for various damping ratio and excitation frequency. Finally, effect of geometry of the micro-beam on the value of phase shifting was studied. It was shown that increasing the geometrical parameter leads to increase the value of phase shifting. Finally, it can be concluded that considering the mentioned parameters in design of phase shifters can be more useful and leads to accurate and high performance designs.

## REFERENCES

- [1] Sallèse J M., Grabinski W., Meyer V., Bassin C., Fazan P., 2001, Electrical modeling of a pressure sensor MOSFET, *Sensors and Actuators A*: **94**: 53-58.
- [2] Nabian A., Rezazadeh G., Haddad derafshi M., Tahmasebi A., 2008, Mechanical behavior of a circular micro plate Subjected to uniform hydrostatic and non-uniform electrostatic pressure, *Journal of Microsystem Technologies* **14**: 235-240.
- [3] Rezazadeh G., Fathalilou M., Shabani R., Tarverdilou S., Talebian S., 2009, Dynamic characteristics and forced response of an electrostatically actuated micro-beam subjected to fluid loading, *Journal of Microsystem Technologies* **15**: 1355-1363.
- [4] Senturia S., 2001, *Microsystem Design*, Kluwer, Norwell, MA, USA.
- [5] Fathalilou M., Motallebi A., Rezazadeh G., Yagubizade H., Shirazi K., Alizadeh Y., 2009, Mechanical behavior of an electrostatically-actuated micro-beam under mechanical shock, *Journal of Solid Mechanics* **1**: 45-57.
- [6] Abdel-Rahman E M., Younis M I., Nayfeh A H., 2002, Characterization of the mechanical behavior of an electrically actuated micro-beam, *Journal of Micromechanics and Microengineering* **12**: 759-766.
- [7] Nayfeh A., Younis M. I., 2005, Dynamics of MEMS resonators under superharmonic and subharmonic excitations, *Journal of Micromechanics and Microengineering* **15**: 1840-1847.
- [8] Younis M. I., Miles R., Jordy D., 2006, Investigation of the response of microstructures under the combined effect of mechanical shock and electrostatic forces, *Journal of Micromechanics and Microengineering* **16**: 2463-2474.
- [9] Rezazadeh G., Fathalilou M., Sadeghi M., 2011, Pull-in voltage of electrostatically-actuated micro-beams in terms of lumped model pull-in voltages using novel design corrective coefficients, *Journal of Sensing and Imaging*, 10.1007/s11220-011-0065-2.
- [10] Shiban K., Bharathi B., 1991, *Microwave and Millimeter Wave Phase Shifters 1*, Boston, Artech House.
- [11] Shiban K., Bharathi B., 1991, *Microwave and Millimeter Wave Phase Shifters 2*, Boston, Artech House.
- [12] Simon JW., Alverson W K., Pippin J E., 1966, A Reciprocal TEM latching ferrite phase shifter, *International Microwave Symposium*, 241-246.
- [13] Garver R V., 1972, Broadband diode phase shifters, *IEEE Transactions on Microwave Theory and Techniques* **20**:658-674.
- [14] Andricos C., Bahi I J., Griffin E L., 1985, C-band 6-bit gas monolithic phase shifter, *IEEE Transactions on Microwave Theory and Techniques* **33**: 1591-1596.
- [15] Vorhous J L., Pucel R A., 1982, Monolithic dual-gate GaAs FET digital phase shifter, *IEEE Transactions on Microwave Theory and Techniques* **30**: 982-992.
- [16] Barker N S., Rebciz G M., 1998, Distributed MEMS true-time delay phase shifters and wide-band switches, *IEEE Transactions on Microwave Theory and Techniques* **46**: 1881-1890.
- [17] Hayden J S., Rebeiz G M., 2003, Very low-loss distributed X-band and Ka-band MEMS phase shifters using metal-air-metal capacitors, *IEEE Transactions on Microwave Theory and Techniques* **51**(1): 309-314.
- [18] Hayden J. S., Rebeiz G. M., 2000, 2-bit MEMS distributed X-band phase shifters, *IEEE Microwave Guided Wave Letters* **10**: 540-542.
- [19] Pillans B., Eshelman S., Malczewski A., Ehmke J., Goldsmith C G., 1999, Ka-band RF MEMS phase shifters, *IEEE Microwave Guided Wave Letters* **9**: 520-522.
- [20] Malczewski A., Eshelman S., Pillans B., Ehmke J., Goldsmith C L., 1999, X-band RF MEMS phase shifters for phased array applications, *IEEE Microwave and Guided Wave Letters* **9**(12): 517-519.
- [21] Younis M I., Abdel-Rahman E M., Nayfeh A., 2003, A Reduced-order model for electrically actuated micro-beam-based MEMS, *Journal of Microelectromechanical Systems* **12**(5):672-680.
- [22] Rezazadeh G., Fathalilou M., Shabani R., 2009, Static and dynamic stabilities of a micro-beam actuated by a piezoelectric voltage, *Journal of Microsystem Technologies* **15** :1785-1791.
- [23] Nayfeh H., Mook, 1979, *Nonlinear Oscillations*, New York, Wiley and Sons.
- [24] Osterberg P M., Senturia S D., 1997, M-TEST: a test chip for MEMS material property measurement using electrostatically actuated test structures, *Journal of Microelectromechanical Systems* **6**:107-118.
- [25] Hung E S., Senturia S D., 1999, Generating efficient dynamical models for microelectromechanical systems from a few finite-element simulation runs, *Journal of Microelectromechanical Systems* **8**: 280-289.